G−1:C73 Recognition by an Arginine Cluster in the Active Site of *Escherichia coli* Histidyl-tRNA Synthetase†

Susan A. Connolly,‡,⊥ Abbey E. Rosen,§,⊥ Karin Musier-Forsyth,*,§ and Christopher S. Francklyn*,‡

Department of Biochemistry, University of Vermont, Health Sciences Complex, Burlington, Vermont, 05405, and Department of Chemistry, University of Minnesota, Minneapolis, Minnesota 55455

Received September 22, 2003; Revised Manuscript Received November 21, 2003

ABSTRACT: Aminoacylation of a transfer RNA (tRNA) by its cognate aminoacyl-tRNA synthetase relies upon the recognition of specific nucleotides as well as conformational features within the tRNA by the synthetase. In *Escherichia coli*, the aminoacylation of $tRNA^{His}$ by histidyl-tRNA synthetase (HisRS) is highly dependent upon the recognition of the unique G−1:C73 base pair and the 5′-monophosphate. This work investigates the RNA−protein interactions between the HisRS active site and these critical recognition elements. A homology model of the $tRNA^{His}$−HisRS complex was generated and used to design site-specific mutants of possible G−1:C73 contacts. Aminoacylation assays were performed with these HisRS mutants and N−1:C73 $tRNA^{His}$ and $microhelix^{His}$ variants. Complete suppression of the negative effect of 5′-phosphate deletion by R123A HisRS, as well as the increased discrimination of Q118E HisRS against a 5′-triphosphate, suggests a possible interaction between the 5′-phosphate and active-site residues Arg123 and Gln118 in which these residues create a sterically and electrostatically favorable pocket for the binding of the negatively charged phosphate group. Additionally, a network of interactions appears likely between G−1 and Arg116, Arg123, and Gln118 because mutation of these residues significantly reduced the sensitivity of HisRS to changes at G−1. Our studies also support an interaction previously proposed between Gln118 and C73. Defining the RNA−protein interactions critical for efficient aminoacylation by *E. coli* HisRS helps to further characterize the active site of this enzyme and improves our understanding of how the unique identity elements in the acceptor stem of $tRNA^{His}$ confer specificity.

Molecular recognition of transfer RNAs by aminoacyl-tRNA synthetases (aaRS)[1] is the obligatory step in protein synthesis that serves to match each amino acid with its three letter nucleotide codon. The determination of the sites on the tRNA that provide recognition by the synthetase has been termed 'tRNA identity'. For many tRNA systems, the important nucleotides that contribute to identity have been reported (*1*−*4*). An important early model in the field was that synthetases bind to the inside edge of the tRNA L-shape (*5*), and later work showed that the anticodon and the acceptor stem serve in many systems as the principal elements of tRNA structures that are recognized by the enzyme (*1*−*4*). However, the three-dimensional context in which these elements are displayed and other more global aspects of tRNA structure, including the tertiary core, have also emerged as being crucial to tRNA identity (*3*, *6*, *7*).

A more difficult problem for which the picture is much less clear is how, precisely, identity elements serve to facilitate recognition. The requirement that tRNAs be efficiently turned over during protein synthesis limits the degree to which binding interactions alone can serve to regulate specificity (*8*, *9*). Hence, a large component of specificity is manifested at steps that follow the binding interaction, and this is reflected in the early observation that discrimination between cognate and noncognate tRNAs relies more heavily on changes in V_{max} than on K_m (*10*). More recently, work in both the glutaminyl and aspartyl systems indicates that, depending on the region of the tRNA they contact, aaRS side chains that interact with tRNA can influence the strength of initial binding, the rate of catalysis, or both (*11*, *12*).

Among all tRNAs, histidine tRNAs are striking for their possession of an extra nucleotide (G−1) present at the 5′-end of the acceptor stem (*13*). Interestingly, histidine tRNAs of prokaryotic origin pair G−1 with a cytosine (conforming to Watson−Crick rules), while eukaryotic tRNAs possess an adenosine at position 73 (*13*). Genes of prokaryotic histidine tRNAs directly encode for the extra guanosine, while a posttranscriptional mechanism operates in eukaryotes to incorporate G−1 (*14*, *15*). The extra guanosine nucleotide imposes specialized requirements for processing of the $tRNA^{His}$ acceptor stem by RNase P (*16*, *17*).

† This work was supported by N. I. H. Grants GM49928 (K.M.-F.) and GM54899 (C.S.F.) and N. I. H. Predoctoral Training Grants T32-GM08700 (A.E.R.) and T32-CA09286 (S.A.C.).

* To whom correspondence should be addressed. Karin Musier-Forsyth: address 207 Pleasant St. SE, Minneapolis, MN 55455, phone (612) 624-0286, fax (612) 626-7541, e-mail musier@chem.umn.edu. Christopher S. Francklyn: address 89 Beaumont Ave., Burlington, VT 05405, phone (802) 656-8450, fax (802) 862-8229, e-mail franck@emba.uvm.edu.

‡ University of Vermont.

§ University of Minnesota.

⊥ S.A.C. and A.E.R. contributed equally to this work.

[1] Abbreviations: aaRS, aminoacyl-tRNA synthetases; xxxRS, specific aminoacyl-tRNA synthetases in which xxx is the three letter code referring to the appropriate amino acid; DTT, dithiothreitol; IPTG, isopropyl 1-thio-β-D-galactopyranoside; Ni-NTA, nickel nitrilotriacetic acid; PCR, polymerase chain reaction; PP_i, inorganic pyrophosphate; TCA, trichloroacetic acid.

10.1021/bi035708f CCC: $27.50
Published on Web 01/09/2004

Kinetic analysis of in vitro transcripts of full-length tRNA first demonstrated that G−1:C73 is an important recognition determinant (*18*), an observation later confirmed by transplantation studies into mini- and microhelices (*19*, *20*). While in vivo amber suppression studies suggested that histidine identity is more dependent on C73 (*21*), the absence of G−1 leads to marked decreases (on the order of 240- to 470-fold) in the aminoacylation of both prokaryotic and yeast tRNAs (*18*, *22*). Other, more recent work suggests that the terminal 5′-phosphate of $tRNA^{His}$ contributes to recognition of G−1 (*23*). The existence of a specific recognition pocket for the 5′-end could also explain the particular sensitivity of histidine tRNA synthetase (HisRS) to the presence of a triphosphate at the 5′-end of full-length and truncated helical substrates (*18*, *19*). In contrast to the acceptor stem, substitutions of the anticodon lead to increases in K_m, but have little effect on V_{max} (*24*, *25*). How these identity elements at both ends of $tRNA^{His}$ confer specificity remains an area of active investigation.

Concurrently with studies on tRNA identity, much effort has been devoted to understanding how subtle distinctions in tRNA synthetase structure mediate differential recognition of tRNAs (*26*). HisRS possesses the two principal domains of the class II aaRS, namely, an N-terminal catalytic domain organized around a six-stranded antiparallel β sheet and a C-terminal anticodon binding domain composed of a mixed parallel/antiparallel β sheet that is topologically related to the nucleotide binding domain (*27*). Insights into how HisRS recognizes its cognate tRNA have come from footprinting experiments (*28*), genetic selection experiments directed against mutant amber suppressors (*25*), and modeling by comparison to other class II aaRS complexes (*27*, *29*, *30*). These data collectively suggest a model in which the tRNA makes principal contacts with the anticodon binding domain and active site cleft of one subunit and minor contacts with the back face of the catalytic domain of the other subunit (*25*, *29*, *30*).

The results of filter binding experiments suggest that initial interactions between the synthetase and the tRNA are dominated by binding interactions with the anticodon (*28*). By contrast, interactions with the acceptor stem C73 determinant contribute little to initial binding contacts (*28*) but exert a predominantly greater effect on steps associated with V_{max} (*18*, *25*). Recent studies utilizing modeling and mutagenesis indicate that residues in the motif 2 loop (particularly the highly conserved glutamine at position 118) strongly contribute to recognition of C73 (*30*). This result is consistent with the hypothesis that the motif 2 loop has a conserved structural and functional role in tRNA recognition in class II aaRSs, a proposal supported by the crystallographic analysis of the complexes of AspRS and SerRS with their cognate tRNAs (*31*, *32*) and by biochemical studies (*33*−*35*).

The present study was undertaken in an effort to identify individual side chains in the active site of *E. coli* HisRS that are important for providing specificity for the unique G−1:C73 base pair. On the basis of a model of the HisRS−$tRNA^{His}$ complex derived by structural superposition with other class II aaRS−tRNA complexes, a cluster of three conserved arginines was identified in the HisRS active site that may contribute to recognition of G−1:C73 in the cognate complex. These candidate residues were subjected to oligonucleotide-directed mutagenesis, and aminoacylation assays with both wild-type and N−1:C73 variant $tRNA^{His}$ and $microhelix^{His}$ substrates were carried out to investigate the consequences of the substitutions for tRNA recognition.

MATERIALS AND METHODS

Reagents, Materials, and General. The nickel nitrilotriacetic acid (Ni-NTA) agarose resin for purification of the His_6−HisRS protein was purchased from QIAGEN. Oligonucleotides for site-directed mutagenesis were obtained from Operon Technologies. Most restriction enzymes and other molecular biology reagents were purchased from New England Biolabs. The *EcoT*221 was obtained from Amersham Biosciences. The ribo- and deoxyribonucleotides were also purchased from Amersham Biosciences, as was the L-[2,5-^{3}H]-histidine. The specific activity of the latter generally ranged from 40 to 70 Ci/mmol. DNA sequencing to confirm the mutations was carried out by the Vermont Cancer Center DNA Sequencing Facility. All solutions were prepared using deionized MilliQ water.

Mutagenesis of Active Site Residues and Production of Mutant Proteins. The construction and purification of Q118E HisRS was described previously (*30*). The HisRS mutants R9H, R116A, and R123A were constructed using the QuikChange system (Stratagene), as described previously (*30*). The starting plasmid for the PCR-based mutagenesis of the gene for histidyl-tRNA synthetase (*hisS*) was pWY30, the construction of which has been described previously (*25*). The primers for mutagenesis were generally 33−36 nucleotides in length and were designed with a predicted melting temperature of 74 °C. All of the mutants were confirmed by sequencing the entire *hisS* gene. Plasmids encoding the mutant proteins were transferred to JM105 for expression and purification, using previously described procedures (*25*, *30*). Fractions containing HisRS from the Ni-NTA column were essentially homogeneous for HisRS and were pooled, concentrated, and dialyzed into storage buffer (100 mM Tris HCl, 100 mM NaCl, 1 mM β-mercaptoethanol, 40% glycerol). The concentration of HisRS was determined by absorbance at 280 nm using an extinction coefficient of 127 097 M^{-1} cm^{-1}, as described in ref *25*. Concentrations determined by absorbance agreed well with those determined by active site titration. Previous studies indicate that the wild-type and His_6-affinity-tagged versions of HisRS exhibit identical kinetic behavior with respect to tRNA.

Construction of Wild-type Full-Length and G-1 Variant $tRNA^{His}$. The synthesis of T7 transcripts based on the sequence of full-length wild-type $tRNA^{His}$ employed the pWY40 plasmid and was accomplished as described previously (*25*). Variants of $tRNA^{His}$ featuring sequence variation at G−1 were constructed from two chemically synthesized oligonucleotides that, when annealed and ligated, reconstitute the 76-nucleotide wild-type tRNA cloverleaf. The choice of the synthetic oligonucleotide approach was motivated by the poor utilization by T7 RNA polymerase of templates initiating with nucleotides other than G (*36*). The overall procedure and several important technical considerations associated with this approach were reported previously (*37*). Synthetic tRNAs were generated by annealing and ligating two oligonucleotides corresponding to nucleotides 1−34 and 35−76 in the mature $tRNA^{His}$ molecule. Following com-

mercial chemical synthesis (Dharmacon, Lafayette, CO), the oligonucleotides were deprotected by treatment with 100 mM acetic acid (pH 3.8) and gel-purified on a denaturing polyacrylamide gel. The 5′-phosphates were introduced by treatment with T4 polynucleotide kinase at a final concentration of 100 U/mL. The oligonucleotides were annealed by heating equimolar ratios of the half-molecules to 70 °C and cooling over a 4-h period to room temperature. Additional cooling to 4 °C was carried out prior to the addition of 15 μg/mL of RNA ligase. Ligation was carried out at 37 °C for 5 h to yield maximal ligation of the half-molecules as assessed by 7 M urea−PAGE. In a typical experiment, ligation efficiencies of 50−75% were achieved, and the full-length molecules were purified away from unligated half-molecules by electrophoresis on denaturing polyacrylamide gels. The less than quantitative ligation efficiency is likely due to the presence of competing structures in one of the two half-molecules; more efficient ligation might be obtained by optimizing the ratio of the two strands (*37*). After isolation from the gel by electroelution, the ligated tRNAs were refolded by heating to 60° and then slow cooling to room temperature in the presence of 1 mM $MgCl_2$. The concentrations of active ligated molecules were determined from aminoacylation plateau experiments.

Microhelix Preparation. All RNA synthesis chemicals, standard bases, and modified bases were purchased from Glen Research (Sterling, VA). Solid-phase synthesis of RNA microhelices was accomplished using the phosphoramidite method on an Expedite 8909 (Applied Biosystems) (*38*, *39*). The microhelix containing 2-aminopurine was synthesized using 2′-*O*-triisopropylsilyloxymethyl (TOM)-protected phosphoramidites (*40*). RNA oligonucleotides were purified on 16% polyacrylamide gels, eluted, and desalted as described (*38*, *39*).

Aminoacylation Assays with tRNAs. In vitro aminoacylation assays were carried out as described previously (*25*). Reaction conditions consisted of 50 mM Hepes (pH 7.5, 25 °C), 20 mM KCl, 8.3 mM DTT, 2.5 mM ATP, 12.5 mM $MgCl_2$, 20 μM histidine, 2.4 μM [^{3}H]-histidine, 0.5−10 μM $tRNA^{His}$, and enzyme concentrations varying from 10 to 100 nM. Reactions (60 μL final volume) were incubated at 37 °C, and then 11 μL aliquots were removed at varying times to derive initial rates. The reaction time points were spotted onto Whatmann 3MM cellulose filters presoaked with 10% TCA and then processed to determine the accumulation of [^{3}H]-histidylated-$tRNA^{His}$ by previously published methods (*19*). Initial rate data were fit to the Michaelis−Menten equation by nonlinear regression as implemented in the KaleidaGraph software package (Synergy software, version 3.08d).

Aminoacylation Assays with Microhelices. RNA microhelices were annealed immediately before use by incubating at 80 °C for 2 min, cooling to 60 °C for 2 min, adding $MgCl_2$ to 10 mM, cooling to 25 °C for 5 min, and placing on ice. Aminoacylation assays were performed at 25 °C as previously described (*19*) in a buffer of 50 mM Hepes (pH 7.5), 20 mM β-mercaptoethanol, 20 mM KCl, 10 mM $MgCl_2$, 4 mM ATP, 20 μM histidine, and 6.2 μM [^{3}H]-histidine. Annealed microhelices (5−20 μM final concentration) and all other assay components were preequilibrated to room temperature before initiation of the reaction by addition of 0.05 μM HisRS or 0.3−0.6 μM mutant HisRS. Initial rates of aminoacylation are proportional to RNA concentration under the conditions used for these experiments. Thus, V_0/[S] is an accurate reflection of k_{cat}/K_m.

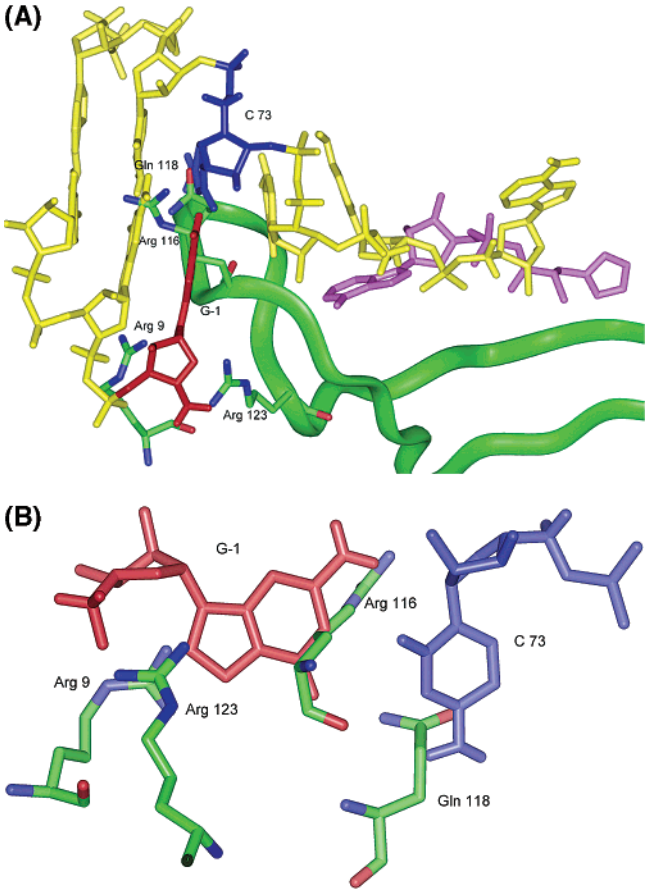

FIGURE 1: Docking model of the HisRS−$tRNA^{His}$ complex: (A) top view; (B) view from the back from active site with the G−1:C73 in a standard Watson−Crick configuration. The HisRS motif 2 loop is rendered in green, the $tRNA^{His}$ acceptor stem is rendered in yellow (G−1 and C73 are colored red and blue, respectively), and the histidyl adenylate is rendered in magenta. HisRS active site residues examined in this study are rendered in stick form and labeled. The tRNA model was derived by substituting $tRNA^{His}$ nucleotides into the structure of uncomplexed $tRNA^{Phe}$ by use of the Biopolymer module of Insight II (MSI, version 98.0). The procedure for superposition of the model complex onto the coordinates of yeast AspRS−$tRNA^{Asp}$ was described previously (*30*). No attempt was made to refine the resulting model by molecular mechanics, and the conformations of individual side chains represent those of the tRNA-free histidyl−adenylate complex (*46*).

RESULTS

Modeling the G-1 Binding Pocket and Identification of Putative G-1 Targets. Although crystal structures of a number of tRNA synthetase−tRNA complexes are available, none of these tRNAs possesses the extra 5′-nucleotide found in $tRNA^{His}$. To formulate specific predictions about the residue(s) in *E. coli* HisRS responsible for contacting the unique 5′-guanosine, the homology model previously constructed to identify potential C73 contacts in $tRNA^{His}$ (*30*) was modified by inclusion of an extra guanosine opposite C73 (Figure 1). For the sake of simplicity, the additional G was positioned to take advantage of potential base stacking with G1 and hydrogen bonding with C73. Because the goal of this exercise was to make qualitative predictions about

Table 1: Steady-State N−1 Discrimination by Active Site *E. Coli* HisRS Mutants[a]

	tRNA^{His}								
	full-length (G−1)			synthetic G−1			synthetic A−1		
HisRS	K_m (μM)	k_{cat} (s^{-1})	k_{cat}/K_m (10^6 M^{-1} s^{-1})	K_m (μM)	k_{cat} (s^{-1})	k_{cat}/K_m (10^6 M^{-1} s^{-1})	K_m (μM)	k_{cat} (s^{-1})	k_{cat}/K_m (10^6 M^{-1} s^{-1})
WT	0.34	2.04	6.0	1.2	4.75	3.9	0.96	0.018	0.02
R9H	15.0	2.54	0.17	17.8	0.76	0.043	15.5	0.024	0.002
R116A	5.8	1.76	0.30	8.13	0.13	0.016	6.3	0.012	0.002
R123A	4.8	0.12	0.03	2.5	0.11	0.044	2.6	0.002	0.0008

[a] Steady-state parameters were determined at 37 °C. The values given above represent at least three separate experiments; standard deviations were within 20% of the above values. Synthetic tRNAs were annealed and ligated to produce the N−1 substituted substrates used in these assays.

likely neighbors and not a detailed quantitative analysis, molecular mechanics and molecular dynamics approaches were not applied, and we did not attempt to explicitly model the likely conformational readjustments of the motif 2 main and side chain elements. As shown in Figure 1, the resulting model nevertheless makes the testable prediction that arginines corresponding to positions 9, 116, and 123 and glutamine 118 are potential contact candidates for the G−1 nucleoside, its 5′-phosphate, or both.

Oligonucleotide mutagenesis was used to construct substitutions of each arginine to either histidine or alanine, resulting in the generation of R9H, R116A, and R123A mutant proteins. These mutant enzymes, along with the Q118E mutant generated previously (*30*), were overexpressed and purified by Ni-NTA affinity chromatography as described in the Materials and Methods section. Each mutant protein accumulated to levels equivalent to the wild-type enzyme and behaved identically to the wild-type with regard to purification. None of the residues substituted appears to play a structural role in HisRS (*27*), so it is assumed that the mutations introduced do not impose any unforeseen local or global structural effects that would complicate the aminoacylation analysis. In support of this conclusion, ATP−PP_i pyrophosphate exchange assays revealed that the mutants possess levels of amino acid activation activity that are indistinguishable with respect to the wild-type enzyme (data not shown).

Aminoacylation Function and Specificity for G-1. To determine whether the active site mutations affected interactions with tRNA, the mutant proteins were first assessed for aminoacylation function using full-length tRNA transcripts. The results of these assays indicated that the mutants were approximately 20- to 200-fold less active than wild-type HisRS. The mutations affected the k_{cat} and K_m aminoacylation parameters to different extents (Table 1). Previously, Q118E was shown to have no effect on K_m and to cause an approximately 7-fold decrease in k_{cat} for aminoacylation of wild-type tRNA^{His} (*30*). For R116A and R9H, the decrease in activity was entirely the result of 17- to 45-fold respective increases in the K_m parameter. By contrast, the R123A mutant exhibited both a 14-fold increase in K_m and a 17-fold decrease in k_{cat}. This suggests that contacts made by Arg123 may be functionally distinct from those of Arg9 or Arg116 and may be more direct with respect to interactions with tRNA^{His}.

Mutant enzyme specificity for the N−1 base was then assessed by comparing aminoacylation catalytic efficiencies of synthetic tRNA^{His} molecules that differed at the −1 position. These synthetic tRNAs were produced by annealing and ligating RNA oligonucleotides corresponding to nucleotides 1−34 and 35−76. In aminoacylation assays carried out with the wild-type enzyme, the ligated G−1 tRNA exhibited a slight 3.5-fold elevated K_m relative to the full-length transcript (Table 1). It is not clear why the tRNAs produced via chemical synthesis exhibit increased Michaelis constants relative to those produced enzymatically, but this result is similar to what was observed with the annealed tRNAs previously studied (*30*).

When G−1 was substituted with A, k_{cat} decreased significantly, leading to a 195-fold overall decrease in k_{cat}/K_m. This effect corresponds to a $-\Delta\Delta G^{\ddagger}$ of ~3.6 kcal/mol, which is comparable to the effect of C73 substitutions (*18*, *30*). Aminoacylation assays were next carried out with the R9H, R116A, and R123A HisRS mutants. The activity ratios ((k_{cat}/K_m G−1)/(k_{cat}/K_m A−1)) for the R9H and R123A mutants (21.5- and 55-fold, respectively) were all less than the 195-fold ratio observed for wild-type HisRS. However, the R116A variant exhibited an activity ratio of only 8-fold, which was the lowest ratio of all of the mutants. These data suggest that this mutant is the least able to discriminate between G−1 and A−1. On the basis of these results, the Arg116 side chain represents the best candidate for direct contact with G−1, although the extent of suppression of the A−1 substitution was modest at best.

Microhelix Studies Identify a Contact with the 5′*-Phosphate of tRNA^{His}*. Microhelices have been previously shown to be useful substrates for HisRS, recapitulating major specificity features despite catalytic efficiencies that are some 200-fold reduced relative to the full-length tRNA (*20*). The direct contribution of the G−1:C73 functional groups to aminoacylation catalytic efficiency has recently been examined in the microhelix^{His} system (Figure 2) (*41*). Briefly, it was found that the exocyclic functional groups of C73 and the 5′-monophosphate each contribute approximately 4 kcal/mol to transition state stability, while the functional groups of G−1 were somewhat less critical to efficient aminoacylation by HisRS. The 6-keto oxygen displayed the largest $-\Delta\Delta G^{\ddagger}$ value of all of the G−1 atomic groups tested (3.1 kcal/mol). In the present study, aminoacylation of microhelix^{His} variants by the HisRS mutants described above was used to further define RNA−protein interactions between the tRNA^{His} G−1:C73 base pair and the HisRS active site. We compared activity ratios ((relative $k_{cat}/K_m{}^{Mut\ HisRS}$)/(relative $k_{cat}/K_m{}^{WT\ HisRS}$), where relative k_{cat}/K_m is that of the microhelix variant relative to the wild-type microhelix), also referred to as suppression efficiencies, to determine possible RNA−protein interactions within the active site. The larger the activity ratio is, the more effective the suppression by

Table 2: Aminoacylation Activity Ratios of Microhelix^{His} Variants and Active Site *E. coli* HisRS Mutants[a]

	micro^{His}						
HisRS	Δ5′-P	U−1:C73	C−1:C73	Ab−1:C73	2AP−1:C73	2AA−1:C73	G−1:A73
WT	1 (−510)	1 (−46)	1 (−310)	1 (−48)	1 (−200)	1 (−580)	1 (−96)
R9H	13	9.1	4.5	5.6	8.8	12	3.6
R116A	17	14	39	9.8	17	29	1.7
R123A	290	45	88	160	71	78	10
Q118E	92	10	49	44	‘9	31	15

[a] Nonstandard bases are abbreviated as follows: Ab, 2′-deoxyabasic; 2AP, 2-aminopurine; 2AA, 2-aminoadenine. Activity ratios are calculated as follows: $((k_{cat}/K_m)^{Mut\ micro}/(k_{cat}/K_m)^{WT\ micro})^{Mut\ HisRS}/((k_{cat}/K_m)^{Mut\ micro}/(k_{cat}/K_m)^{WT\ micro})^{WT\ HisRS}$. Values are the result of at least four trials with an average standard deviation of ±32%. Numbers in parentheses are fold-decreases in k_{cat}/K_m of the indicated variant relative to wild-type microhelix^{His}.

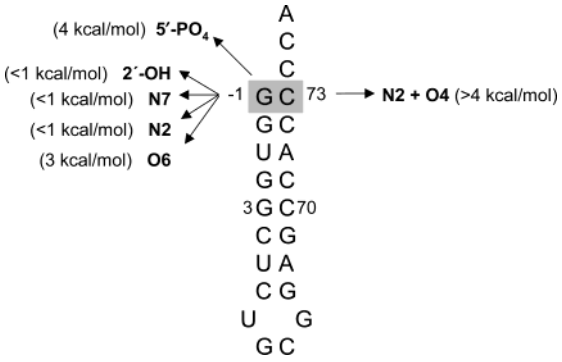

FIGURE 2: Sequence of microhelix^{His} used in aminoacylation assays. The G−1:C73 base pair is shaded and arrows point to atomic groups that were previously tested for their contribution to aminoacylation catalytic efficiency; $-\Delta\Delta G^{\ddagger}$ values are indicated in parentheses ($-\Delta\Delta G^{\ddagger} = RT \ln(k_{cat}/K_m)^{mutant}/(k_{cat}/K_m)^{wild-type}$; $R = 1.982$ 72 cal/(mol·K); $T = 298$ K).

the HisRS mutant of the defect introduced by a microhelix^{His} variant is. A high suppression efficiency is equivalent to a loss of discrimination between the mutated functional group and that of the wild-type sequence. Interactions identified in this manner are good candidates for direct contacts between the HisRS side chain and the G−1:C73 base pair.

We first determined the effect of the HisRS point mutations on aminoacylation of wild-type microhelix^{His}. The R9H and R116A mutations resulted in approximately 670 (±200)-fold decreases in k_{cat}/K_m. The R123A and Q118E changes had even larger effects of −2300 (±800)-fold and −5700 (±1800)-fold, respectively. The much larger magnitude of these effects compared to the decreases observed with the full-length tRNA (7- to 200-fold) (ref *30* and Table 1) likely reflect the differences in binding energy between the microhelix and full-length tRNA substrates.

Prior studies indicate that the 5′-phosphate constitutes an important recognition element that is even more critical than the functional groups of the G−1 base itself (*18*, *23*, *41*) (Figure 2). To determine the site of interaction between HisRS and the 5′-monophosphate, a microhelix^{His} variant lacking this critical functional group (Δ5′-P) was chemically synthesized. Comparison of the activities of the wild-type and mutant HisRSs with Δ5′-P microhelix^{His}, indicated that among the mutant proteins the R9H and R116A enzymes remained the most sensitive to the loss of the 5′-phosphate, as suggested by the smaller values for the activity ratios (Table 2). By contrast, the R123A and Q118E mutants were significantly less sensitive to the absence of the 5′-phosphate than the wild-type enzyme, R123A HisRS exhibiting an activity ratio of 290, representing the highest value of all of the mutant enzymes. As shown in Figure 3, the R123A HisRS mutation resulted in essentially complete suppression of the Δ5′-P effect. The activity ratio of 92 measured with Q118E HisRS was the second highest value and represents partial suppression of the Δ5′-P defect. Hence, Arg123 and Gln118 both represent potential residues that are in contact with the 5′-phosphate of microhelix^{His}, Arg123 being an excellent candidate for a direct interaction.

To provide further confirmation of the role of these residues in 5′-phosphate recognition in the context of full-length tRNA^{His}, the aminoacylation of wild-type tRNA^{His} transcripts containing a 5′-triphosphate by the wild-type and the four mutant proteins was investigated. Previously, an inhibitory effect of a triphosphate on the 5′-end of tRNA^{His} and minihelix^{His} transcripts had been reported (*18*, *19*). As reported in Table 3, these experiments showed that discrimination against the 5′-triphosphate decreases from nearly 4-fold in the case of wild-type HisRS to less than 2-fold in the case of R123A HisRS. A similar 2-fold level of discrimination was seen for R9H, while R116A exhibited a 6-fold discrimination against the triphosphate. The most striking result was obtained with Q118E, which exhibited a 17-fold discrimination against the triphosphate. These results are consistent with the hypothesis that local electrostatic interactions between the motif 2 loop and the 5′-end of the tRNA are critical. The reduced level of discrimination seen with R123A and R9H suggests that removal of these side chains facilitates the positioning of the extra phosphate moieties in the active site; this effect would be balanced by the loss of a basic charge to neutralize the additional negative charges from the phosphate. By contrast, the Q118E mutation creates an additional local negative charge, and the resulting electrostatic repulsion imposes a $-\Delta\Delta G^{\ddagger}$ of nearly 1.7 kcal/mol. Thus, studies with the full-length 5′-triphosphate tRNA^{His} support the hypothesis that both Arg123 and Gln118 are critical for interactions with the 5′-base pair of tRNA^{His}.

G-1 Functional Group Analysis by Use of Microhelix Substrates. The aminoacylation of microhelix^{His} substrates containing N−1:C73 base pair mutations with the HisRS variants provided additional evidence for contacts between G−1 and active site residues. Aminoacylation of the U−1:C73 and C−1:C73 microhelix^{His} variants with R116A, R123A, and Q118E gave significant activity ratios (*10*−*88*), indicating a loss of sensitivity to the identity of the −1 base. In contrast, R9H HisRS had lower activity ratios of 9.1 and 4.5 for U−1 and C−1 microhelices, respectively. Similar trends were observed when the dAbasic−1:C73, 2-aminopurine:C73, and 2-aminoadenosine−1:C73 microhelices were aminoacylated with the HisRS mutants. These results suggest that Arg116, Arg123, and Gln118 may all contribute either

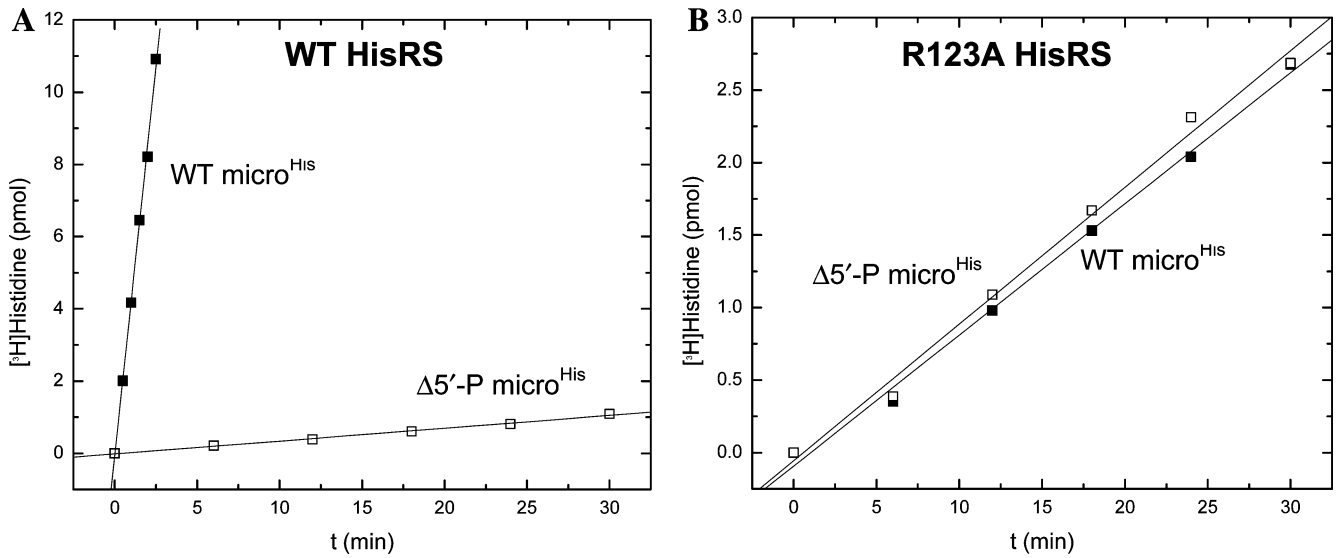

FIGURE 3: Aminoacylation of wild-type (■) and Δ5′-P (□) microhelix^{His} with (A) wild-type HisRS and (B) R123A HisRS.

Table 3: Discrimination against 5′-Triphosphate on tRNA^{His} by Wild-type and Mutant HisRS[a]

HisRS	5′-PO$_4$ k_{cat}/K_m (M^{-1} s^{-1})	5′-PPP k_{cat}/K_m (M^{-1} s^{-1})	discrimination ratio
WT	5.4×10^6	1.4×10^6	3.8
R9H	7.5×10^4	3.6×10^4	2.1
R116A	1.7×10^5	2.7×10^4	6.3
R123A	4.1×10^4	2.2×10^4	1.8
Q118E	1.6×10^4	9.3×10^2	17

[a] Values were determined from the initial rates of aminoacylation at 37 °C, pH 7.5, using tRNA substrate concentrations of 0.1 μM for wild-type tRNA^{His} and 0.5 μM for ppp-tRNA^{His}, which are well below K_m. Each value represents the average of 2−3 independent determinations. Standard deviations in the measurements were typically ±25%.

directly or indirectly to recognition of G−1, but Arg9 is considerably less likely to do so.

The G−1:A73 microhelix^{His} variant allowed investigation of C73 discrimination. As previously reported, Gln118 is likely to contact C73 (*30*), and the activity ratio of 15 measured for aminoacylation of the G−1:A73 variant by Q118E HisRS supports this conclusion. R123A HisRS exhibited an activity ratio of 10 with G−1:A73 microhelix^{His} (as compared to 3.6 and 1.7 for R9H and R116A, respectively), suggesting an intermediate effect. However, this value represents the lowest suppression efficiency measured for R123A HisRS and thus is likely to represent an indirect effect at best. The lower activity ratios observed with R9H and R116A HisRS suggest that these residues are not likely to be in direct contact with C73.

DISCUSSION

The unique G−1 extra nucleotide that all histidine tRNAs possess distinguishes them from all other tRNAs. Extensive prior studies indicate that G−1:C73 serves both to mark histidine tRNAs as substrates for HisRS and discourages interactions with noncognate tRNA synthetases (*18*, *19*, *42*). It would appear that the requirement for specific aminoacylation by HisRS provides strong principal selective pressure to maintain the G−1 element. Notably, its presence in prokaryotes imposes additional special constraints on processing by RNase P (*16*, *17*), and its presence in eukaryotes requires the posttranscriptional action of a dedicated nucleotidyl transferase (*14*, *15*).

The studies here were undertaken to identify specific side chains on HisRS responsible for recognition of the G−1:C73 base pair and its critical 5′-phosphate. The key findings emerging from our study are that a pair of active site arginines (Arg116 and Arg123), as well as the prokaryotic conserved Gln118, plays a significant role in the recognition of the 5′-end of *E. coli* tRNA^{His}. The third arginine, Arg9, may participate in an electrostatic interaction in the complex but does not appear to be specifically associated with direct recognition of G−1 or the histidine tRNA 5′-phosphate group.

A modified docking model of the HisRS−tRNA^{His} complex (*30*) shows that the three arginines investigated here are located close to G−1 in two different secondary structure elements (Figure 1). These elements are close to the predicted position of the incoming tRNA and, more importantly, could potentially contribute to the formation of a specific pocket for the G−1 base. Arg9 is located at a bend in the polypeptide chain between the N-terminal tail and the first α-helical element of motif 1 in a conserved R/KG-patch (*27*, *43*). This residue is universally an arginine or a lysine, indicating the requirement for a conserved basic charge but not for the guanidinium group in particular. Arg116 and Arg123 are both located in motif 2, one of the class II signature sequences. All HisRSs possess an arginine (prokaryote) or Gln/Asn (eukaryote) at position 116, and the arginine at position 123 is strictly conserved in all HisRS sequences from all three kingdoms (*43*, *44*). Thus, this cluster of basic charges is highly conserved, particularly in prokaryotes. By contrast, the active sites of other class II synthetases for which structures of the complexes with tRNA are available do not possess such pockets (*31*, *32*, *45*), and discrimination against tRNAs with 5′-triphosphates or hydroxyl groups has not been reported (*3*). Thus, a relatively tight interaction with the 5′-end of the tRNA may be specific to HisRS.

These studies also suggest that none of the three arginines is required for the adenylation reaction. Crystal structures of the HisRS histidinol−ATP and histidyl−adenylate com-

plexes showed that Arg121 and Glu115 in the motif 2 loop participate in ATP binding in the first step of the reaction (*27*, *46*). By contrast, there is no structural evidence that Arg116, Gln118, or Arg123 participate in contacts to ATP, and this likely accounts for the absence of an effect by the mutations on the pyrophosphate exchange reaction (data not shown) (*30*). In the motif 2 loops of other class II aaRSs, there are numerous examples of polar side chains the function of which is limited to interactions with tRNA (*12*, *31*, *32*), so this is not unexpected. Accordingly, the location of the three arginines in the structure, their high degree of conservation, and the data presented here are all consistent with the proposed tRNA binding function.

Previous work suggested that binding interactions between HisRS and its cognate tRNA are dominated by contacts to the anticodon, as opposed to the discriminator base (*25*, *28*). The 20- to 200-fold decreases in $tRNA^{His}$ aminoacylation activity associated with the substitution of Arg9, 116, and 123, were reflected largely in the K_m parameter, yet the R123 mutation additionally affected k_{cat} (Table 1). If tRNA binding is in fast exchange relative to the rate of the transfer step, then $K_m \approx K_D$, and the mutations might be expected to increase the overall equilibrium dissociation constant. Thus, the side chains examined here might play more significant roles in binding steps versus catalytic steps. A second significant observation is that substitution of R123 and Q118 brought about a more significant suppression of the loss of the −1 phosphate (Table 2 and Figure 3) than suppression of the decrease associated with the substitution of G at −1 (Tables 1 and 2). In contrast, substitution of R9 and R116 had more similar effects on suppression (Table 2). Previous measurements estimate the contribution of the −1 phosphate of $tRNA^{His}$ to transition state stabilization to be 3.48 kcal/mol (*23*). A recent study using $microhelix^{His}$ variants supports this conclusion (Figure 2) (*41*). This contribution has not been broken down into its specific binding and chemistry components. The complete and partial suppression of the loss of the −1 phosphate by R123 and Q118, respectively, as well as the altered discrimination against a triphosphate at −1, suggest that these residues play significant and perhaps direct roles in the recognition of the 5′-end of the tRNA. This result is similar to an arginine−phosphate interaction previously identified between NADPH and the NADPH−cytochrome P-450 oxidoreductase (*47*). In addition to expected steric effects, the local electrostatic environment is also important in recognition. These data support the argument that the −1 phosphate group contributes more binding free energy than the identity of the −1 nucleotide, but further work will be necessary to more carefully dissect the contribution of the 5′-phosphate to the elementary steps of binding and aminoacyl transfer.

A Multistep Model for Recognition of $tRNA^{His}$. The most completely described class II system with respect to tRNA recognition is the aspartyl system, for which numerous homologous and heterologous AspRS−$tRNA^{Asp}$ crystallographic complexes have been reported (*31*, *48*−*50*). Work on AspRS and its complexes with tRNA suggests that an important intermediate in aminoacylation may be an initial "encounter complex" between the aaRS and the tRNA that is dominated by interactions with the anticodon arm. In the initial encounter complex, direct recognition of functional groups in the acceptor stem may be minimal with the CCA end existing in a structurally disordered state. This state would closely resemble a heterologous complex, such as the one formed between *E. coli* AspRS and yeast $tRNA^{Asp}$ (*50*). The process of cognate aminoacylation following the formation of the encounter complex would likely entail the subsequent docking of the acceptor stem to maximize direct contact with nucleobase functional groups, as well as with the phosphodiester backbone. Positioning of the A76 terminal nucleotide would also have to occur prior to the actual chemical transfer step, perhaps by virtue of conformational rearrangement of the flipping loop or structural equivalent (*49*).

Although such a model is based in part on inferences derived from analysis of heterologous complexes, a number of the results reported here and elsewhere for HisRS are consistent with this picture. In particular, it has been shown that mutations in the $tRNA^{His}$ anticodon have a clear effect on the binding step (*28*) but little effect on the rate of transfer under single-turnover conditions (S. H. Connolly and C. S. Francklyn, unpublished results). By contrast, mutations at the discriminator base have no effect on the tRNA equilibrium dissociation constant (*28*) and lead to preferential decreases in the k_{cat} for aminoacylation (*18*, *25*). With respect to the data reported here, it is noteworthy that in the context of the wild-type full-length $tRNA^{His}$, the substitutions of the three different arginines exhibited distinctly different kinetics effects (Table 1) with the R123A substitution affecting both K_m and k_{cat}. Taken together with the conclusion that Arg123 plays a major role in recognition of the 5′-phosphate (Table 2), these results suggest that positioning of the 5′-terminus may be particularly important for subsequent rate-determining steps in aminoacylation, including adjustment of the CCA end. Indeed, Fromant et al argued that the contact to the 5′-phosphate is more important than the direct interactions with the nucleobase (*23*).

As indicated by the suppression ratios of 45−160 and 10−39 reported in Table 2 for the R123A and R116A mutant proteins, respectively, these variants along with Q118E appeared to exhibit a marked decrease in their ability to discriminate among different nucleobases at the −1 position (Table 2). This effect was significantly enhanced in the context of microhelices relative to the effect noted with the full-length tRNA (Table 1). This apparent discrepancy may reflect the greater amount of binding energy available to the enzyme upon interaction with the full-length tRNA substrate relative to the microhelix substrate, a difference that might tend to accentuate the individual free energy contribution of a contact between the enzyme and nucleobase functional group in the context of a microhelix (*51*).

Comparisons between the effects mediated by different −1:73 base combinations are also subject to the contributions of structural effects on the RNA mediated by mutant base pairs. Nevertheless, our results suggest that Arg123 is likely to comprise part of a network of contacts that also includes Gln118, the productive interaction of which with G−1:C73 may be necessary for the correct positioning of the CCA end, perhaps by virtue of fostering motif 2 flipping loop interactions. More structural work will be needed to further define this model. Along these lines, the conformational effect of the unique G−1 base in $microhelix^{His}$ has recently been examined by NMR (*52*). Deletion of G−1 results in fraying of the first two base pairs in the acceptor stem and

a much less well-defined conformation of the CCA 3′ end, which assumes a stacked, fold-back conformation in the wild-type microhelix^{His}. If, as we believe, the unique conformation of the acceptor stem end of tRNA^{His} contributes to induced fit binding of the CCA end trinucleotide, this could account for the importance of the active site residues identified in this work and rationalize their role in the discrimination between cognate and noncognate tRNAs.

REFERENCES

1. McClain, W. H. (1995) in *tRNA: Structure, Biosynthesis, and Function* (Söll, D., and RajBhandary, U., Eds.) pp 335−347, ASM Press, Washington, DC.
2. Pallanck, L., Pak, M., and Schulman, L. H. (1995) in *tRNA: Structure, Biosynthesis, and Function* (Söll, D., and RajBhandary, U. L., Eds.) pp 371−394, ASM Press, Washington, DC.
3. Giegé, R., Sissler, M., and Florentz, C. (1998) *Nucleic Acids Res. 26*, 5017−5035.
4. Beuning, P. J., and Musier-Forsyth, K. (1999) *Biopolymers 52*, 1−28.
5. Rich, A., and Schimmel, P. R. (1977) *Nucleic Acids Res. 4*, 1649−1665.
6. Christian, T., Lipman, R. S. A., Evilia, C., and Hou, Y.-M. (2000) *J. Mol. Biol. 303*, 503−514.
7. Sherlin, L. D., Bullock, T. L., Newberry, K. J., Lipman, R. S. A., Hou, Y.-M., Beijer, B., Sproat, B. S., and Perona, J. J. (2000) *J. Mol. Biol. 299*, 431−446.
8. Schimmel, P. R., and Söll, D. (1979) *Annu. Rev. Biochem. 48*, 601−648.
9. Schimmel, P. (1987) *Annu. Rev. Biochem. 56*, 125−158.
10. Ebel, J. P., Giegé, R., Bonnet, J., Kern, D., Befort, N., Bollack, C., Fasiolo, F., Gangloff, J., and Dirheimer, G. (1973) *Biochimie 55*, 547−557.
11. Sherman, J. M., Thomann, H. U., and Söll, D. (1996) *J. Mol. Biol. 256*, 818−828.
12. Eriani, G., and Gangloff, J. (1999) *J. Mol. Biol. 291*, 761−773.
13. Sprinzl, M., Horn, C., Brown, M., Ioudovitch, A., and Steinberg, S. (1998) *Nucleic Acids Res. 26*, 148−153.
14. Cooley, L., Appel, B., and Söll, D. (1982) *Proc. Natl. Acad. Sci. U.S.A. 79*, 6475−6479.
15. L'Abbe, D., Lang, B. F., Desjardins, P., and Morais, R. (1990) *J. Biol. Chem. 265*, 2988−2992.
16. Burkard, U., Willis, I., and Söll, D. (1988) *J. Biol. Chem. 263*, 2447−2451.
17. Green, C. J., and Vold, B. S. (1988) *J. Biol. Chem. 263*, 652−657.
18. Himeno, H., Hasegawa, T., Ueda, T., Watanabe, K., Miura, K.-I., and Shimizu, M. (1989) *Nucleic Acids Res. 17*, 7855−7863.
19. Francklyn, C., and Schimmel, P. (1990) *Proc. Natl. Acad. Sci. U.S.A. 87*, 8655−8659.
20. Francklyn, C., Shi, J.-P., and Schimmel, P. (1992) *Science 255*, 1121−1125.
21. Yan, W., and Francklyn, C. (1994) *J. Biol. Chem. 269*, 1−7.
22. Rudinger, J., Florentz, C., and Giegé, R. (1994) *Nucleic Acids Res. 22*, 5031−5037.
23. Fromant, M., Plateau, P., and Blanquet, S. (2000) *Biochemistry 39*, 4062−4067.
24. Nameki, N., Asahara, H., Shimizu, M., Okada, N., and Himeno, H. (1995) *Nucleic Acids Res. 23*, 389−394.
25. Yan, W., Augustine, J., and Francklyn, C. (1996) *Biochemistry 35*, 6559−6568.
26. Arnez, J. G., and Moras, D. (1994) in *RNA-Protein Interactions* (Nagai, K., and Mattaj, I. W., Eds.) pp 52−81, Oxford University Press, Oxford, U.K.
27. Arnez, J. G., Harris, D. C., Mitschler, A., Rees, B., Francklyn, C. S., and Moras, D. (1995) *EMBO J. 14*, 4143−4155.
28. Bovee, M. L., Yan, W., Sproat, B. S., and Francklyn, C. S. (1999) *Biochemistry 38*, 13725−13735.
29. Åberg, A., Yaremchuck, A., Tukalo, M., Rasmussen, B., and Cusack, S. (1997) *Biochemistry 36*, 3084−3094.
30. Hawko, S. A., and Francklyn, C. S. (2001) *Biochemistry 40*, 1930−1936.
31. Cavarelli, J., Eriani, G., Rees, B., Ruff, M., Boeglin, M., Mitschler, A., Martin, F., Gangloff, J., Thierry, J.-C., and Moras, D. (1994) *EMBO J. 13*, 327−337.
32. Cusack, S., Yaremchuk, A., and Tukalo, M. (1996) *EMBO J. 15*, 2834−2842.
33. Davis, M., Buechter, D., and Schimmel, P. (1994) *Biochemistry 33*, 9904−9911.
34. Lenhard, B., Landeka, I., and Söll, D. (1997) *J. Biol. Chem. 272*, 1136−1141.
35. Burke, B., Yang, F., Chen, F., Stehlin, C., Chan, B., and Musier-Forsyth, K. (2000) *Biochemistry 39*, 15540−15547.
36. Milligan, J. F., and Uhlenbeck, O. C. (1989) *Methods Enzymol. 180*, 51−62.
37. Pleiss, J. A., Wolfson, A. D., and Uhlenbeck, O. C. (2000) *Biochemistry 39*, 8250−8258.
38. Scaringe, S. A., Francklyn, C., and Usman, N. (1990) *Nucleic Acids Res. 18*, 5433−5441.
39. Sproat, B., Colonna, F., Mullah, B., Tsou, D., Andrus, A., Hampel, A., and Vinayak, R. (1995) *Nucleosides Nucleotides 14*, 255−273.
40. Wu, X., and Pitsch, S. (1998) *Nucleic Acids Res. 26*, 4315−4323.
41. Rosen, A. E., and Musier-Forsyth, K. (2003) *J. Am. Chem. Soc.*, in press.
42. Yan, W., and Francklyn, C. (1995) *Nucleic Acids Symp. Ser.*, 167−169.
43. Ruhlmann, A., Cramer, F., and Englisch, U. (1997) *Biochem. Biophys. Res. Commun. 237*, 192−201.
44. Francklyn, C., Adams, J., and Augustine, J. (1998) *J. Mol. Biol. 280*, 847−858.
45. Sankaranarayanan, R., Dock-Bregeon, A.-C., Romby, P., Caillet, J., Springer, M., Rees, B., Ehresmann, C., Ehresmann, B., and Moras, D. (1999) *Cell 97*, 371−381.
46. Arnez, J. G., and Moras, D. (1997) *Trends Biochem. Sci. 22*, 211−216.
47. Sem, D. S., and Kasper, C. B. (1993) *Biochemistry 32*, 11548−11558.
48. Ruff, M., Krishnaswamy, S., Boeglin, M., Poterszman, A., Mitschler, A., Podjarny, A., Rees, B., Thierry, J. C., and Moras, D. (1991) *Science 252*, 1682−1689.
49. Eiler, S., Dock-Bregeon, A., Moulinier, L., Thierry, J. C., and Moras, D. (1999) *EMBO J. 18*, 6532−6541.
50. Moulinier, L., Eiler, S., Eriani, G., Gangloff, J., Thierry, J. C., Gabriel, K., McClain, W. H., and Moras, D. (2001) *EMBO J. 20*, 5290−5301.
51. Saks, M. E., and Sampson, J. R. (1996) *EMBO J. 15*, 2843−2849.
52. Seetharamen, M., Williams, C., Cramer, C., and Musier-Forsyth, K. (2003) *Nucleic Acids Res. 31*, in press.

BI035708F